

Low-Reynolds number aerodynamic response of a NACA0012 airfoil in oscillatory motion

Baris Gungordu^{1,*} and Berk Tayfuner²

¹Aerospace Engineering, Middle East Technical University, Northern Cyprus Campus, Güzelyurt via Mersin 10, 99738 Kalkanlı, Türkiye

²Berlin School of Business & Innovation, Artificial Intelligence, 12043 Berlin, Germany

Abstract. Unsteady aerodynamic phenomena associated with plunging and pitching airfoils are of great importance in understanding biological flight, energy harvesting, and next-generation unmanned aerial systems. While numerous studies have explored these mechanisms at low Reynolds numbers, there remains a gap in systematically linking validated low-Re experiments to higher Reynolds regimes using high-fidelity numerical methods.

In this study, we investigate the unsteady lift and drag behaviour of a NACA 0012 airfoil undergoing pure pitch and pure plunge motions. An incompressible 2-D flow model is developed in OpenFOAM and validated against well-established low Reynolds number ($Re \approx 1000$) benchmark cases from the literature for static cases. The developed framework achieved a high accuracy ($\approx 95\%$) across angle-of-attacks between $1-30^\circ$. The computational setup reproduces key parameters such as lift and drag coefficients, allowing direct comparison with existing experimental and numerical data.

After successful validation, the Reynolds number is kept constant to examine emerging flow features for pitching and plunging motion, such as wake deflection, vortex shedding patterns, and their impact on aerodynamic performance. The results highlight how unsteady aerodynamic benefits evolve pure pitching and plunging modes, providing valuable insight for efficient propulsion and flow-control strategies for the future studies.

1 Introduction

The pure pitching and plunging motions of airfoils have been extensively studied over the past three decades [1, 2]. Flapping airfoils in various configurations have been investigated to mimic bio-inspired flight mechanisms observed in hummingbirds, insects, and other small flyers. Beyond biological inspiration, combined pitching and plunging motions are also of interest for aerodynamic flow control, as they can enhance the performance and efficiency of unmanned aerial vehicles (UAVs) and small-scale aircraft [3, 4]. Lai and Platzer investigated NACA0012 airfoil that was sinusoidally plunging and conducted water-tunnel tests showing that the oscillations yielded a thrust force [5]. In addition, Sarkar has observed a trailing-edge vortex pattern opposite of the expected Von Karman vortex street indicating that there is a thrust force [6]. Cleaver *et al.* experimentally examined small-amplitude sinusoidal plunge oscillations of a NACA0012 airfoil at post-stall angles of attack and demonstrated that the lift coefficient increases linearly with the plunge velocity [7]. More recently, Gursul and Cleaver further investigated plunging oscillations of airfoils and finite wings, showing that the formation of leading-edge vortices contributes to increased mean thrust and lift forces [8]. Sev-

eral computational studies are conducted by the development of commercial flow solvers with prescribed pitching/plunging motion [9, 10].

In this paper, a physics-based model, which does not rely on any prescribed motion, is employed within the OpenFOAM framework to numerically investigate the pure pitching and pure plunging motions of a NACA0012 airfoil. The formulation allows the airfoil dynamics to evolve naturally under the fluid–structure interaction rather than being imposed through predefined kinematics. The study focuses on three distinct angles of attack for both motion modes, analyzed separately across free-stream Reynolds numbers of 1,000, 5,000, and 10,000. This approach enables a systematic comparison of unsteady aerodynamic responses under varying flow regimes, offering insights into the effect of reduced frequency and Reynolds number on lift generation, vortex development, and flow stability characteristics.

After this brief introduction, the paper is organized as follows. Section 2 describes the numerical methods and the validation of the computational model. Section 3 presents the results and discussions. Finally, Section 4 provides the conclusions and future work of the study.

*Corresponding author: gbaris@metu.edu.tr

2 Numerical Methods and Validation

This paper utilises an numerical approach using OpenFOAM to study NACA0012 airfoil's pure pitching and plunging motions. For the validation of the numerical model Reynolds number, $Re = 1000$ is used to solve incompressible Reynolds-Averaged Navier-Stokes equation over the NACA0012 airfoil. The airfoil has a chord length of 0.1 m and a free-stream velocity of 0.146 ms^{-1} to obtain $Re = 1000$ as per the reference validation study. The turbulence model is $k-\omega$ SST with PISO pressure correction.

Figure 1 presents the physical model that consists of two springs namely the axial spring for pitching and vertical spring for plunging.

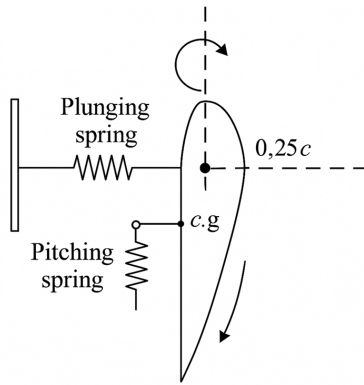


Figure 1. Physical model with vertical and axial springs.

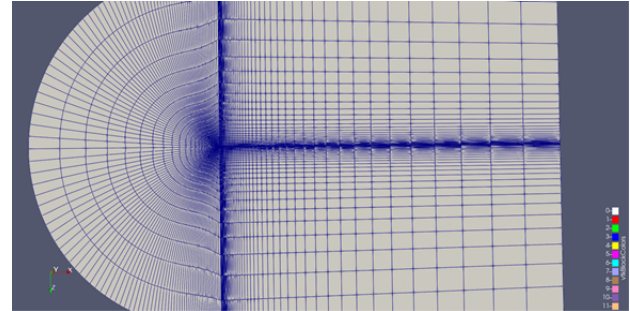
A structured hexahedral C-type mesh was generated in blockMesh for the computational domain surrounding the NACA0012 airfoil. The domain extends 100 chord lengths upstream and downstream, and 50 chord lengths above and below the airfoil to minimize far-field effects. Mesh refinement was applied in both the streamwise and normal directions using graded cell distributions. The refinement ratio was 30,000 in the wall-normal direction to accurately capture the boundary layer. The mesh was verified using the checkMesh utility to ensure quality within acceptable limits. Table 1 summarizes the key properties of the mesh used in this study.

Table 1. Summary of mesh properties.

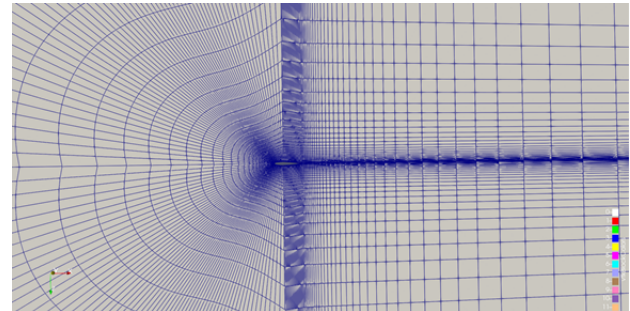
| Property | Value | Description |
|-----------------------|--------------------------------|---|
| Domain size | 200×100 | 100 chord lengths upstream and downstream |
| Cell type | Hexahedral | Structured blocks |
| Total cells | $\sim 2.7 \times 10^5$ | Computational elements in 3D domain |
| Minimum cell size | 0.002 | Near airfoil surface |
| Δx_{\min} | | |
| Maximum skewness | 0.45 | Within recommended limit (< 0.5) |
| First layer thickness | $1.2 \times 10^{-5} \text{ m}$ | Wall-adjacent cell height |
| y_1 | | |
| Average y^+ | 0.8 | Satisfies viscous sublayer resolution ($y^+ \approx 1$) |

The overall mesh quality was satisfactory for the intended low Reynolds number simulations. The maximum

skewness and non-orthogonality values remained below the recommended limits for steady and transient RANS analyses. The first cell height corresponded to $y^+ \approx 1$, ensuring full resolution of the viscous sublayer without employing wall functions. Mesh independence was confirmed by comparing aerodynamic coefficients for progressively refined grids. Figure 2 presents a visualisation of C-type mesh and a magnified view to present the airfoil.



(a)



(b)

Figure 2. Mesh visualisation (a) Full-domain (b) Magnified view of airfoil.

Initially, the airfoil studied without pitching/plunging motions to obtain validation of the so-called static OpenFOAM model is made with Kurtulus [11] and shown in Figure 3. It is shown that the numerical model of the present study has captured the lift coefficient (C_l) of the reference paper with a high accuracy.

The airfoil motion was simulated using the *three-degree-of-freedom (3-DoF)* solver in OpenFOAM, coupled with a distance-based mesh deformation method to preserve cell quality near the moving surface. The body mass was set to 10 kg, with the center of gravity located at $(0.4198, -0.0146, 0)$ and principal moments of inertia $(0.845, 1.667, 1.458) \text{ kg} \cdot \text{m}^2$. The initial orientation corresponded to a 1° rotation about the z -axis and zero angular momentum. The motion was constrained to *pure pitching* about the quarter-chord point ($0.25c$) by fixing the pivot location and allowing rotation only around the z -axis. A linear angular spring-damper with stiffness $k_\theta = 57.6 \text{ N} \cdot \text{m}/\text{rad}$ and damping $c_\theta = 0.18 \text{ N} \cdot \text{m} \cdot \text{s}/\text{rad}$ (natural frequency $\approx 1 \text{ Hz}$, damping ratio $\zeta \approx 0.001$) provided the restoring torque. The rigid-body equations were integrated using the *symplectic* time-integration scheme,

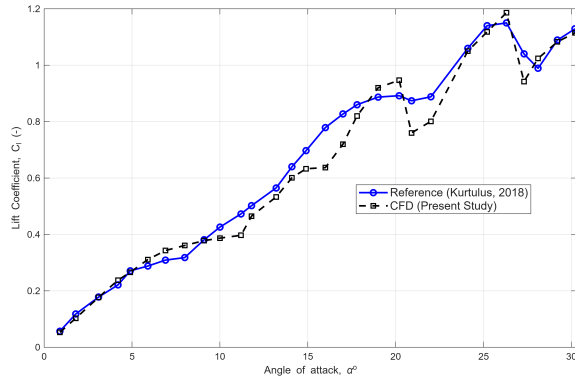


Figure 3. C_l versus α for the static model compared with reference study

with constant fluid density $\rho_\infty = 1.225 \text{ kg/m}^3$ and gravity neglected. The time step of the simulation is set to 1×10^{-4} and the total computational time for each case is 300 seconds. To calculate the average lift and drag coefficients first 60 seconds of the data is disregarded.

Equation 1 presents the instantaneous pure-pitching mode's angle-of-attack change with the sinusoidal input in which the α_0 is the initial angle-of-attack, $\hat{\alpha}$ is the amplitude and f is the oscillation frequency.

$$\alpha(t) = \alpha_0 + \hat{\alpha} \sin(2\pi ft) \quad \text{about the } 0.25c \text{ pivot.} \quad (1)$$

Equation 2 describes the pure-plunging mode's motion with the sinusoidal input. In the equation, \hat{h} is the plunging amplitude and h_0 is the initial position which is equal to α_0 for all cases presented in this paper.

$$h(t) = h_0 + \hat{h} \sin(2\pi ft) \quad (2)$$

Equation 3 presents the instantaneous lift coefficient ($C_l(t)$) showing the sinusoidal modes implemented for the pitching and plunging motion modes in which the \hat{C}_l is the time-averaged lift coefficient

$$C_l(t) = \bar{C}_l + \hat{C}_l \sin(2\pi ft + \phi) \quad (3)$$

3 Results and Discussions

In this section, the numerical results are presented for pure pitching and plunging. The Reynolds number of the flow is kept constant at $Re = 1000$ throughout the section.

3.1 Pure Pitching Motion

The first set of simulations examines *pure* pitching of the airfoil. The axial spring is configured to produce a harmonic rotation of amplitude 1° at 1 Hz for all cases, while the mean incidence is set to three representative values, $\alpha_0 = 4.9^\circ$, 19.0° , and 26.3° , corresponding to low, moderate, and high angles of attack. Figure 4 shows the transient response for $\alpha_0 = 4.9^\circ$: the lift coefficient oscillates nearly sinusoidally, as expected from the imposed kinematics, with a cycle-averaged value of $\bar{C}_l = 0.225$. The

reference solution for the same case reports $C_l \approx 0.228$, yielding a small deviation of 1.3%, which supports the fidelity of the present set-up.

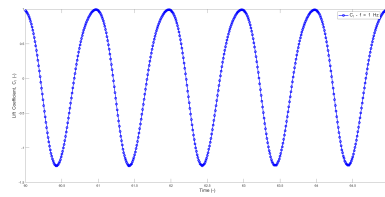


Figure 4. Time-domain solutions of lift coefficient for $f = 1 \text{ Hz}$.

Table 2 summarises the time-averaged lift and its percentage change relative to the stationary baseline. At low and moderate α_0 , the mean lift remains close to the static values (changes of -0.44% and -3.3%), indicating that a small pitch amplitude (1°) primarily introduces phase-lagged fluctuations without producing a significant bias in the cycle average. At the highest incidence (26.3°), \bar{C}_l is reduced by 13.7%. This trend is consistent with a picture in which small-amplitude pitching modulates the separated shear layer and intermittently weakens the leading-edge suction during parts of the cycle, so that the net contribution over one period is slightly negative. In short, with fixed frequency and a modest pitch amplitude, pitching acts mainly as a kinematic perturbation: it preserves the mean lift at low and moderate angles but tends to decrease it in deep stall, in agreement with the behaviour reported in the reference study [11].

Table 2. Pure pitching results: time-averaged lift and percentage change relative to the stationary baseline.

| α_0 ($^\circ$) | \bar{C}_l | ΔC_l (%) |
|-------------------------|-------------|------------------|
| 4.9 | 0.225 | -0.44 |
| 19.0 | 0.858 | -3.3 |
| 26.3 | 0.437 | -13.7 |

Figure 5 presents the flow visualisation of velocity field for pure-pitching. Figure 5a shows the initial case when $t = 0$ and Figure 5b presents the velocity field when the airfoil was fully pitched up showing the trailing edge vortices.

The drag coefficient decreases on average by 29.5% across three cases which increases the overall aerodynamic efficiency.

3.2 Pure Plunging Motion

For the pure plunging cases, the heave amplitude is set to $h_0 = 0.5c$ and the motion is sinusoidal at 1 Hz, matching the pitching tests. Table 3 summarises the time-averaged lift coefficients, \bar{C}_l , and the percentage change relative to the stationary baseline. The data show a clear lift augmentation with plunging across all three mean angles of attack: \bar{C}_l rises to 0.648 at $\alpha_0 = 4.9^\circ$ (+143.6%), to 1.322

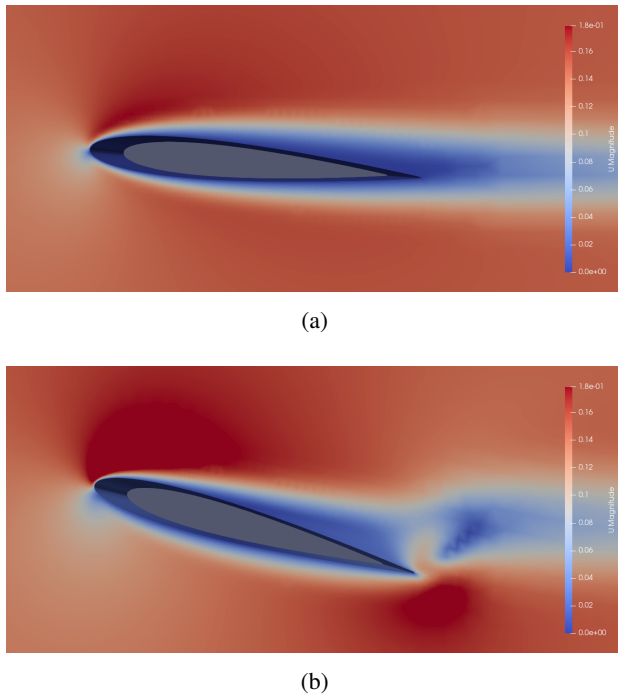


Figure 5. Velocity field visualization of the pitching motion: (a) initial position, (b) maximum pitch-up position.

at $\alpha_0 = 19.0^\circ$ (+48.8%), and to 1.705 at $\alpha_0 = 26.3^\circ$ (+43.8%).

These trends are consistent with the expected unsteady mechanisms. The vertical velocity of the section increases the effective angle of attack, $\alpha_{\text{eff}}(t) = \alpha_0 + \tan^{-1}(\dot{h}/U_\infty)$, yielding a positive bias in lift over a cycle. At the larger amplitude used here ($h_0 = 0.5c$), added-mass and circulatory contributions are substantial, and periodic formation of a leading-edge vortex during the downstroke further strengthens suction on the upper surface. The relative gain is largest at the low mean angle (4.9°), where the baseline flow is largely attached and the heave-induced \dot{h}/U_∞ provides an outsized increment in effective incidence. As α_0 increases into post-stall conditions, plunging still enhances the mean lift by promoting intermittent reattachment and vortex lift, but the percentage gain diminishes because the baseline \bar{C}_l is already elevated and the separated shear layer limits further improvement. Overall, the monotonic increase of \bar{C}_l with α_0 together with decreasing relative increments aligns with a picture in which heave primarily augments lift via effective-angle modulation at low α_0 and via controlled leading-edge vortex dynamics at higher α_0 .

Table 3. Pure *plunging* results: time-averaged lift and percentage change relative to the stationary baseline.

| α_0 ($^\circ$) | \bar{C}_l | Δ (%) |
|-------------------------|-------------|--------------|
| 4.9 | 0.535 | 101.1 |
| 19.0 | 1.413 | 39.3 |
| 26.3 | 1.552 | 30.8 |

Figure 6 presents the flow visualisation of velocity field for pure-plunging. Figure 6a shows the half way plunge-up (initial case when $t = 0$ is the same as Figure 5a) and Figure 6b presents the velocity field when the airfoil was fully pitched up presenting both leading edge and trailing edge vortices.

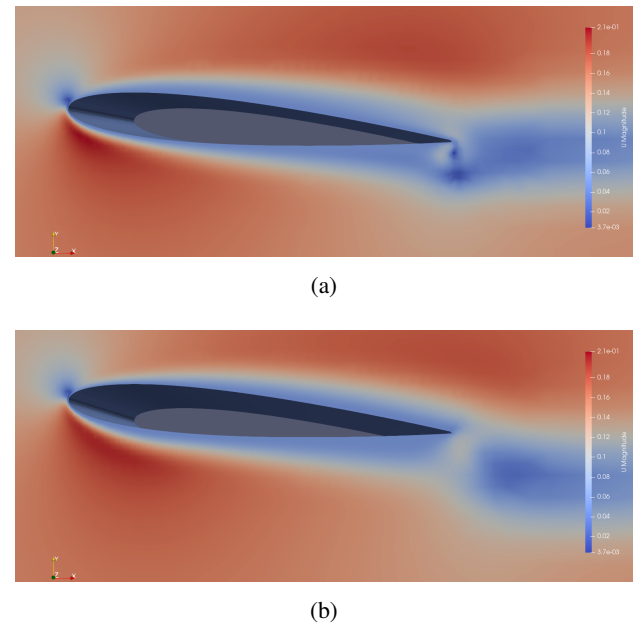


Figure 6. Velocity field visualization of the plunging motion: (a) mid-plunge position, (b) uppermost position of the cycle.

Although the drag coefficient increases by an average of 18.3% across the three cases, the overall aerodynamic efficiency is still improved.

4 Conclusions

In this study, the unsteady lift and drag behaviour of a NACA0012 airfoil undergoing pure pitching and pure plunging motions was numerically investigated. An incompressible two-dimensional flow model was developed in OpenFOAM and validated against well-established low Reynolds number ($Re \approx 1000$) benchmark cases for static conditions. The developed framework demonstrated high accuracy of C_l computation ($\approx 95\%$) across angles of attack between 1° and 30° , successfully reproducing key aerodynamic parameters such as lift and drag coefficients in agreement with existing experimental and numerical data.

The validated model was then applied to analyse the effects of unsteady motion on aerodynamic performance. For pure pitching, small-amplitude oscillations (1° at 1 Hz) induced sinusoidal fluctuations in lift without significant change in the time-averaged value, while at high angles of attack a slight reduction in mean lift was observed due to transient weakening of the leading-edge suction. In contrast, the pure plunging cases ($h_0 = 0.5c$, 1 Hz) produced a marked increase in time-averaged lift across

all studied incidences. This enhancement was attributed to the modulation of effective angle of attack, added-mass effects, and the periodic formation of leading-edge vortices that intensified upper-surface suction.

Overall, the results confirm that plunging motion substantially augments lift compared with static and pitching cases, particularly at moderate angles of attack. The developed numerical framework provides a robust basis for studying unsteady aerodynamic mechanisms and can be extended to coupled pitch–plunge or phase-shifted motion configurations. **For future work**, the same approach will be extended to investigate higher Reynolds numbers (e.g., $Re = 10,000$ and above) to explore the transition from laminar to transitional flow regimes and assess the persistence of the observed trends under more realistic aerodynamic conditions for future aeronautical flow control applications.

References

- [1] H. Hamdani, M. Sun, Aerodynamic forces and flow structures of an airfoil in some unsteady motions at small reynolds number, *Acta Mechanica* **145**, 173 (2000).
- [2] I.H. Tuncer, M. Kaya, Optimization of flapping airfoils for maximum thrust and propulsive efficiency (2003)
- [3] M. Karásek, M. Percin, T. Cunis, B.W. van Oudheusden, C.D. Wagter, B.D. Remes, G.C. de Croon, Accurate position control of a flapping-wing robot enabling free-flight flow visualisation in a wind tunnel, *International Journal of Micro Air Vehicles* **11**, 1756829319833683 (2019), <https://doi.org/10.1177/1756829319833683>. [10.1177/1756829319833683](https://doi.org/10.1177/1756829319833683)
- [4] B. Anılr, D.F. Kurtulus, Numerical Investigation of Sinusoidally Plunging NACA0012 Airfoil at $Re = 1000$ (2023), <https://www.researchgate.net/publication/373639579>
- [5] J.C. Lai, M.F. Platzer, Jet characteristics of a plunging airfoil, *AIAA journal* **37**, 1529 (1999). [10.2514/2.641](https://doi.org/10.2514/2.641)
- [6] S. Sarkar, Comparing pure-pitch and pure-plunge kinematics for a symmetric airfoil (2010), Vol. 48, pp. 2962–2969, ISSN 00011452
- [7] D.J. Cleaver, Z. Wang, I. Gursul, M.R. Visbal, Lift enhancement by means of small-amplitude airfoil oscillations at low reynolds numbers, *AIAA Journal* **49**, 2018 (2011). [10.2514/1.J051014](https://doi.org/10.2514/1.J051014)
- [8] I. Gursul, D. Cleaver, Plunging oscillations of airfoils and wings: Progress, opportunities, and challenges, *AIAA Journal* **57**, 3648 (2019). [10.2514/1.J056655](https://doi.org/10.2514/1.J056655)
- [9] M.S.U. Khalid, I. Akhtar, N.I. Durrani, Analysis of strouhal number based equivalence of pitching and plunging airfoils and wake deflection, *Proceedings of the Institution of Mechanical Engineers, Part G: Journal of Aerospace Engineering* **229**, 1423 (2015). [10.1177/0954410014551847](https://doi.org/10.1177/0954410014551847)
- [10] D.F. Kurtulus, Unsteady aerodynamics of a pitching naca 0012 airfoil at low reynolds number, *International Journal of Micro Air Vehicles* **11** (2019). [10.1177/1756829319890609](https://doi.org/10.1177/1756829319890609)
- [11] D.F. Kurtulus, Aerodynamic loads of small-amplitude pitching naca 0012 airfoil at reynolds number of 1000, *AIAA Journal* **56**, 3328 (2018). [10.2514/1.J056879](https://doi.org/10.2514/1.J056879)